J. Appl. Comput. Mech., 8(4) (2022) 1467-1479
DOI: 10.22055/jacm.2022.40276.3550

ISSN: 2383-4536
jacm.scu.ac.ir

Shahid Chamran University of Ahvaz

Journal of Applied and Computational Mechanics

Research Paper

Comparative Study of Hybrid Lattice Boltzmann and Vorticity-vector Potential Modelling of 2D and 3D Natural Convection Combined with Rosseland Radiation

Alexander Nee

Research and Educational Center of I.N. Butakov, National Research Tomsk Polytechnic University, Tomsk, Russia

Received March 12 2022; Revised June 11 2022; Accepted for publication June 14 2022.
Corresponding author: A. Nee (nee_alexander@mail.ru)

Abstract. This study deals with numerical simulation of two-dimensional and three-dimensional natural convection in a closed differentially heated cube filled with radiatively participating medium. To examine fluid flow and heat transfer, hybrid mesomacroscopic model was developed. Rosseland radiation model was used to determine radiative heat flux. The effect of the Rayleigh number and radiation parameter on temperature, flow pattern and mean convective Nusselt numbers was discussed in detail. It was found that thermal radiation reduced the convective heat transfer rate by around 50% when radiation parameter is increased from 0 to 4. One-cellular quasi two-dimensional flow pattern was formed when taking into account Rosseland radiation. An oblique thermal stratification was formed as the radiation was enhanced. 2D and 3D models under consideration reproduced the same values of temperatures whereas a discrepancy was revealed in velocity components. Convective mean Nusselt numbers were in a very good agreement for both pure finite difference and hybrid lattice Boltzmann simulations with an error less than 5%. Volumetric radiation lowers the time needed to reach steady-state solution by around 60% when Rayleigh number is equal to 10^5. Numerical performance of hybrid lattice Boltzmann method was more than 7 times higher than conventional voriticity-vector potential formulation.

Keywords: BGK approximation, vorticity-vector potential, volumetric radiation, D3Q19 scheme.

1. Introduction

The last few decades combined heat transfer problems via natural convection and radiation received great attention. This phenomenon is encountered in many engineering applications such as photovoltaics, solar collectors, microelectronic cooling etc. Numerical studies are predominantly conducted for differentially heated square cavities [1–10]. Akiyama and Chong [1] solved a combined problem of natural convection and surface thermal radiation in an air-filled domain with vertical isothermal and horizontal adiabatic walls. The authors considered steady two-dimensional flow of viscous incompressible fluid under the Boussinesq approximation. Bouafia et al. [2] solved a similar problem for compressible fluid with temperature-dependent thermophysical properties. While studies [1, 2] were performed for domains with vertically-oriented heat sources, steady and unsteady modes of convective-radiative heat transfer were analyzed in [4] for cavities heated from below.

Analysis of heat transfer by natural convection and volumetric radiation is performed under two-dimensional and three-dimensional problem formulations. Ibrahim and Lemonnier [11] examined a complex heat and mass transfer for a cavity filled with nitrogen and carbon dioxide when the Rayleigh number was equal to 9.2×10^6. Navier-Stokes, diffusion and energy equations were solved in Aquilon. Lari et al. [10] analyzed a similar problem for an optical thickness range of $0 \le \tau_\lambda \le 100$. Borjini et al. [12] considered a differentially heated cubic cavity filled with $LiNbO_3$ melt when Ra = 10^5. Cherifi et al. [13] solved a three-dimensional problem of heat and mass transfer in a domain filled with the mixture of air-H_2O and air-CO_2. The effect of thermal radiation on 3D magnetoconvection and 3D double diffusive convection are studied in [14, 15].

Studies of convective-radiative heat transfer regularities in inclined cavities are conducted for engineering applications predominantly associated with solar collectors. Vivek et al. [16] solved a coupled problem of natural convection and surface thermal radiation under an inclination angle range of $-90° \le \gamma \le 90°$. Moufekkir et al. [17] considered a similar problem taking into account mass transfer.

It is well-known [18–20] that insertions of various shapes modify the flow pattern in cavities. Liu and Phan-Thien [18] analyzed a convective-radiative heat transfer in a differentially heated cavity with a heated block. The effect of radiation on natural convection was studied in [19] under conditions of non-uniform temperature distribution along the heat source. Saravanan and Sivaraj [19] considered a square cavity filled with a radiatively non-participating medium. More detailed analysis of the effect of protrusion shape and its position on convective-radiative heat transfer regularities was performed in [20].

Published online: June 25 2022

Protrusions were fixed at the bottom and/or top horizontal walls and moved along the *X*-axis.

Xin et al. [21] analyzed turbulent natural convection in a differentially heated cavity with horizontal adiabatic walls of finite thickness. Sheremet and Martyushev [22] solved a two-dimensional problem of convective-radiative heat transfer in a square cavity bounded by finite thickness walls and filled with diathermic fluid. An isothermal heat source was fixed at the bottom wall. Later authors [23] numerically examined the heat transfer by laminar natural convection and surface thermal radiation in a cubic domain with isothermal hot plate located at the bottom wall.

Presented works highlighted state of the art problems of natural convection and radiation interaction in closed cavities. The literature review showed that studies of convective-radiative heat transfer are predominantly performed with conventional macroscopic computational fluid dynamics (CFD) techniques for two-dimensional cavities. On the other hand, an alternative CFD tool called the lattice Boltzmann method (LBM) is extensively developed where the medium is considered on the mesoscopic level. The LBM [24, 25] has numerous advantages over conventional CFD approaches based on finite difference, control volume and other numerical techniques. However, the lattice Boltzmann method lacks numerical stability in some cases when solving thermal problems. To overcome this limitation, Lallemand and Lou [26] suggested to implement a hybrid formulation (HLB) instead of widespread double distribution function (DDF) approach. Despite a higher numerical stability and less memory consumption of the HLB in comparison with the DDF, the hybrid lattice Boltzmann scheme is rarely used. By now, volumetric radiation-natural convection coupling via HLB was studied only for two-dimensional cavity [27]. On the other hand, three-dimensional hybrid lattice Boltzmann models are developed for pure natural convection [28] with acoustic wave propagation [29]. To the best of the author knowledge, there is a significant gap in the hybrid lattice Boltzmann simulation of heat transfer and fluid flow. Little papers are published on combined heat transfer by three-dimensional natural convection and radiation analysis in terms of the numerically efficient HLB. Previously [30], the author developed the hybrid lattice Boltzmann scheme for 3D natural convection-surface radiation coupling in order to fill this important research gap. The novelty of the present work is a HLB model for interaction analysis of volumetric radiation and 3D natural convection. Within this hybrid model, numerical procedure for fluid flow will be considered in terms of the lattice Boltzmann method whereas unsteady three-dimensional energy equation will be solved by the finite difference technique.

2. Problem Formulation

2.1 Physical and geometrical models

A closed cube (Fig. 1) with two vertical opposite isothermal walls and heat insulated boundaries is considered. It is assumed that the medium can absorb thermal radiation. Thermophysical properties of fluid were temperature-independent. Natural convective flow was unsteady, three-dimensional and laminar. Fluid assumed to be viscous, heat-conductive, incompressible and Newtonian.

2.2 Lattice Boltzmann formulation

The lattice Boltzmann equation discretized in terms of the Bhatnagar-Gross-Krook (BGK) approximation and D3Q19 stencil is as follows:

$$f_k\left(\vec{x}+\vec{c}_k\cdot\Delta t,\, t+\Delta t\right)=f_k\left(\vec{x},\, t\right)+\Delta t\cdot\xi\cdot\left[f_k^{eq}\left(\vec{x},\, t\right)-f_k\left(\vec{x},\, t\right)\right]+\Delta t\cdot F_k\,. \tag{1}$$

The equilibrium distribution function, macroscopic density and velocity, relaxation frequency and force term are given as:

$$f_k^{eq}=w_k\cdot\rho\cdot\left[1+\frac{\left(\vec{c}_k\cdot\vec{u}\right)}{c_s^2}+\frac{\left(\vec{c}_k\cdot\vec{u}\right)^2}{2\cdot c_s^4}-\frac{\left(\vec{u}\cdot\vec{u}\right)}{2\cdot c_s^2}\right], \tag{2}$$

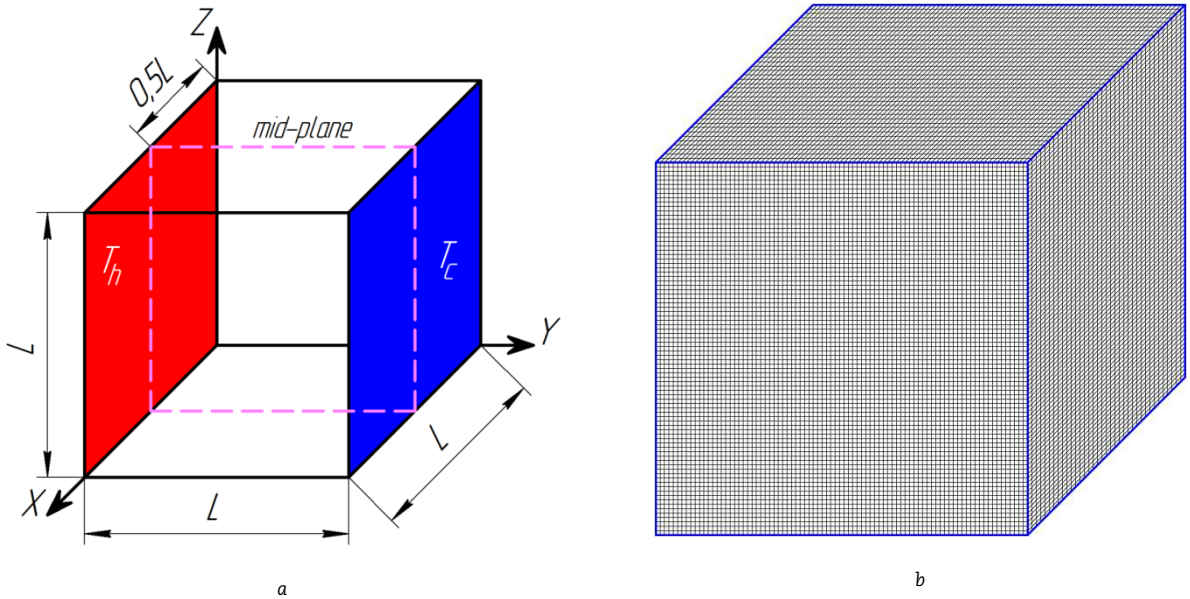

Fig. 1. Physical (a) and computational (b) domains.

$$\rho = \sum_{k=1}^{19} f_k \,, \tag{3}$$

$$\vec{u} = \frac{1}{\rho} \cdot \sum_{k=1}^{19} c_k \cdot f_k \,, \tag{4}$$

$$\xi = \frac{1}{3 \cdot \nu + 0.5} \,, \tag{5}$$

$$F_k = \frac{w_k \cdot \beta \cdot g \cdot \left(T - \frac{T_h + T_c}{2} \right) \cdot c_z}{c_s^2} \,. \tag{6}$$

2.3 Vorticity-vector potential formulation

Heat transfer and fluid flow characteristics obtained with the hybrid lattice Boltzmann model will be compared with the data calculated by conventional finite difference technique. Dimensionless vorticity–vector potential formulation was used to simulate 3D natural convection combined with volumetric radiation. The governing macroscopic equations under Boussinesq approximation are as follows [31, 32]:

$$\frac{\partial \Omega_x}{\partial \tau} + U\frac{\partial \Omega_x}{\partial X} + V\frac{\partial \Omega_x}{\partial Y} + W\frac{\partial \Omega_x}{\partial Z} - \Omega_x\frac{\partial U}{\partial X} - \Omega_y\frac{\partial U}{\partial Y} - \Omega_z\frac{\partial U}{\partial Z} = \sqrt{\frac{\mathrm{Pr}}{\mathrm{Ra}}} \cdot \left(\frac{\partial^2 \Omega_x}{\partial X^2} + \frac{\partial^2 \Omega_x}{\partial Y^2} + \frac{\partial^2 \Omega_x}{\partial Z^2} \right) + \frac{\partial \Theta}{\partial Y} \,, \tag{7}$$

$$\frac{\partial \Omega_y}{\partial \tau} + U\frac{\partial \Omega_y}{\partial X} + V\frac{\partial \Omega_y}{\partial Y} + W\frac{\partial \Omega_y}{\partial Z} - \Omega_x\frac{\partial V}{\partial X} - \Omega_y\frac{\partial V}{\partial Y} - \Omega_z\frac{\partial V}{\partial Z} = \sqrt{\frac{\mathrm{Pr}}{\mathrm{Ra}}} \cdot \left(\frac{\partial^2 \Omega_y}{\partial X^2} + \frac{\partial^2 \Omega_y}{\partial Y^2} + \frac{\partial^2 \Omega_y}{\partial Z^2} \right) - \frac{\partial \Theta}{\partial X} \,, \tag{8}$$

$$\frac{\partial \Omega_z}{\partial \tau} + U\frac{\partial \Omega_z}{\partial X} + V\frac{\partial \Omega_z}{\partial Y} + W\frac{\partial \Omega_z}{\partial Z} - \Omega_x\frac{\partial W}{\partial X} - \Omega_y\frac{\partial W}{\partial Y} - \Omega_z\frac{\partial W}{\partial Z} = \sqrt{\frac{\mathrm{Pr}}{\mathrm{Ra}}} \cdot \left(\frac{\partial^2 \Omega_z}{\partial X^2} + \frac{\partial^2 \Omega_z}{\partial Y^2} + \frac{\partial^2 \Omega_z}{\partial Z^2} \right) \,, \tag{9}$$

$$\frac{\partial^2 \Psi_x}{\partial X^2} + \frac{\partial^2 \Psi_x}{\partial Y^2} + \frac{\partial^2 \Psi_x}{\partial Z^2} = -\Omega_x \,, \tag{10}$$

$$\frac{\partial^2 \Psi_y}{\partial X^2} + \frac{\partial^2 \Psi_y}{\partial Y^2} + \frac{\partial^2 \Psi_y}{\partial Z^2} = -\Omega_y \,, \tag{11}$$

$$\frac{\partial^2 \Psi_z}{\partial X^2} + \frac{\partial^2 \Psi_z}{\partial Y^2} + \frac{\partial^2 \Psi_z}{\partial Z^2} = -\Omega_z \,. \tag{12}$$

Velocity and vector potential are related as follows:

$$U = \frac{\partial \Psi_z}{\partial Y} - \frac{\partial \Psi_y}{\partial Z}; \quad V = \frac{\partial \Psi_x}{\partial Z} - \frac{\partial \Psi_z}{\partial X}; \quad W = \frac{\partial \Psi_y}{\partial X} - \frac{\partial \Psi_x}{\partial Y}.$$

Vorticity and velocity are related as follows:

$$\Omega_x = \frac{\partial W}{\partial Y} - \frac{\partial V}{\partial Z}; \quad \Omega_y = \frac{\partial U}{\partial Z} - \frac{\partial W}{\partial X}; \quad \Omega_z = \frac{\partial V}{\partial X} - \frac{\partial U}{\partial Y}.$$

In order to make equation (7) – (12) dimensionless, the following relations were used:

$$\tau = \frac{t}{t_0}; \quad X = \frac{x}{L}; \; Y = \frac{y}{L}; \quad Z = \frac{z}{L}; \quad U = \frac{u}{V_{nc}}; \; V = \frac{v}{V_{nc}}; \quad W = \frac{w}{V_{nc}}; \; \Theta = \frac{T - T_c}{T_h - T_c}; \; \Omega_x = \frac{\omega_x}{\omega_0}; \quad \Omega_y = \frac{\omega_y}{\omega_0}; \quad \Omega_z = \frac{\omega_z}{\omega_0}; \quad \Psi_x = \frac{\psi_x}{\psi_0};$$

$$\Psi_y = \frac{\psi_y}{\psi_0}; \; \Psi_z = \frac{\psi_z}{\psi_0}; \; V_{nc} = \sqrt{g \cdot \beta \cdot (T_h - T_c) \cdot L}; \quad T_0 = \frac{T_h + T_c}{2}; \; t_0 = L / \sqrt{g \cdot \beta \cdot (T_h - T_c) \cdot L}; \; \psi_0 = V_{nc} L; \; \omega_0 = \frac{V_{nc}}{L}.$$

2.4 Heat transfer formulation

When neglecting the viscous energy dissipation, unsteady three-dimensional energy equation with volumetric radiation under Rosseland approximation is as follows [33, 34]:

$$\frac{\partial \Theta}{\partial \tau} + U\frac{\partial \Theta}{\partial X} + V\frac{\partial \Theta}{\partial Y} + W\frac{\partial \Theta}{\partial Z} = \left(1 + \frac{4}{3} \cdot Rd \right) \frac{1}{\sqrt{Ra \cdot Pr}} \left(\frac{\partial^2 \Theta}{\partial X^2} + \frac{\partial^2 \Theta}{\partial Y^2} + \frac{\partial^2 \Theta}{\partial Z^2} \right). \tag{13}$$

where $Rd = [4 \cdot \sigma \cdot (T_h - T_c)^3] / [\lambda \cdot a_R]$ is radiation parameter, $Ra = [g \cdot \beta \cdot (T_h - T_c) \cdot L^3] / [\nu \cdot a]$ is Rayleigh number, $Pr = \nu / a$ is Prandtl number.

To estimate the heat transfer rate, mean convective Nusselt number at the hot wall was determined as:

$$Nu = \int_0^1 \int_0^1 \left.\frac{\partial \Theta}{\partial Y}\right|_{Y=0} dX \cdot dZ.$$

2.5 Initial and boundary conditions

It was assumed that the fluid was motionless in the initial moment of time:

$$f(X,Y,Z,0) = f^{eq}(X,Y,Z,0),$$

$$\rho(X,Y,Z,0) = 1,$$

$$\Omega_x(X,Y,Z,0) = \Omega_y(X,Y,Z,0) = \Omega_z(X,Y,Z,0) = 0,$$

$$U(X,Y,Z,0) = V(X,Y,Z,0) = W(X,Y,Z,0) = 0,$$

$$\Psi_x(X,Y,Z,0) = \Psi_y(X,Y,Z,0) = \Psi_z(X,Y,Z,0) = 0,$$

$$\Theta(X,Y,Z,0) = 0.5.$$

Boundary conditions for the differentially heated closed cavity are as follows:
at the plane of $Y = 0, 0 < X < 1, 0 < Z < 1$:

$$\Psi_x = \frac{\partial \Psi_y}{\partial Y} = \Psi_z = 0,$$

$$\Omega_x = -\frac{\partial^2 \Psi_x}{\partial Y^2}, \Omega_y = 0, \Omega_z = -\frac{\partial^2 \Psi_z}{\partial Y^2},$$

$$\Theta = 1.$$

at the plane of $Y = 1, 0 < X < 1, 0 < Z < 1$:

$$\Psi_x = \frac{\partial \Psi_y}{\partial Y} = \Psi_z = 0,$$

$$\Omega_x = -\frac{\partial^2 \Psi_x}{\partial Y^2}, \Omega_y = 0, \Omega_z = -\frac{\partial^2 \Psi_z}{\partial Y^2},$$

$$\Theta = 0.$$

at the planes of $X = 0, X = 1, 0 < Y < 1, 0 < Z < 1$:

$$\frac{\partial \Psi_x}{\partial X} = \Psi_y = \Psi_z = 0,$$

$$\Omega_x = 0, \Omega_y = -\frac{\partial^2 \Psi_y}{\partial X^2}, \Omega_z = -\frac{\partial^2 \Psi_z}{\partial X^2},$$

$$\frac{\partial \Theta}{\partial X} = 0.$$

at the planes of $Z = 0, Z = 1, 0 < X < 1, 0 < Y < 1$:

$$\Psi_x = \Psi_y = \frac{\partial \Psi_z}{\partial Z} = 0,$$

$$\Omega_x = -\frac{\partial^2 \Psi_x}{\partial Z^2}, \Omega_y = -\frac{\partial^2 \Psi_y}{\partial Z^2}, \Omega_z = 0,$$

$$\frac{\partial \Theta}{\partial Z} = 0.$$

In order to obtain the value of distribution function at the solid walls, the bounce back condition was applied [35].

2.6 Numerical procedure

Solution algorithm of the lattice Boltzmann method generally consists of two steps such as particles collision and propagation in accordance with equation (1) and $f_k(x+c_k\cdot\Delta t,\, t+\Delta t)=f_k(x,t)$, respectively. After that, no-slip boundary condition is computed using the bounce-back hypothesis and macroscopic density (Eq. 3) and velocity (Eq. 4) of fluid are recovered. On the other hand, the governing partial differential equations (7) – (13) were solved by means of the finite difference method. In order to approximate unsteady three-dimensional equations, the locally one-dimensional implicit scheme of Samarskii [36] was applied. In accordance with this scheme, one time step is performed in three stages. On the first stage ($d\tau/3$), local heat transfer and fluid flow characteristics are computed along the X-axis (Eq. 14). On the second stage ($2d\tau/3$), vorticity, vector potential and temperature are calculated along the Y-axis (Eq. 15). Finally ($3d\tau/3$), required values are determined along the Z-axis (Eq. 16). It should be noted that convective terms were discretized by the second order monotonic scheme of Samarskii [36] whereas the central differences were used to approximate diffusive terms. The governing equations discretized the above were reduced to the standard tridiagonal form and solved by the sweep method [37]. In accordance with the finite difference schemes used in this study, for example, the partial differential equation (13) can be written in discretized form as follows:

$$\frac{\Theta^{n+\frac{1}{3}}_{i,j,k}-\Theta^{n}_{i,j,k}}{d\tau}+U^{n}_{i,j,k}\cdot\frac{\Theta^{n+\frac{1}{3}}_{i+1,j,k}-\Theta^{n+\frac{1}{3}}_{i-1,j,k}}{2\cdot h_x}-\left|U^{n}_{i,j,k}\right|\cdot\frac{\Theta^{n+\frac{1}{3}}_{i+1,j,k}-2\cdot\Theta^{n+\frac{1}{3}}_{i,j,k}+\Theta^{n+\frac{1}{3}}_{i-1,j,k}}{2\cdot h_x}=\frac{1}{\sqrt{\mathrm{Ra}\cdot\mathrm{Pr}}}\left[\left(1+\left|U^{n}_{i,j,k}\right|\cdot\frac{\sqrt{\mathrm{Ra}\cdot\mathrm{Pr}}\cdot h_x}{2}\right)^{-1}\frac{\Theta^{n+\frac{1}{3}}_{i+1,j,k}-2\cdot\Theta^{n+\frac{1}{3}}_{i,j,k}+\Theta^{n+\frac{1}{3}}_{i-1,j,k}}{h_x^2}\right], \tag{14}$$

$$\frac{\Theta^{n+\frac{2}{3}}_{i,j,k}-\Theta^{n+\frac{1}{3}}_{i,j,k}}{d\tau}+V^{n}_{i,j,k}\cdot\frac{\Theta^{n+\frac{2}{3}}_{i,j+1,k}-\Theta^{n+\frac{2}{3}}_{i,j-1,k}}{2\cdot h_y}-\left|V^{n}_{i,j,k}\right|\cdot\frac{\Theta^{n+\frac{2}{3}}_{i,j+1,k}-2\cdot\Theta^{n+\frac{2}{3}}_{i,j,k}+\Theta^{n+\frac{2}{3}}_{i,j-1,k}}{2\cdot h_y}=\frac{1}{\sqrt{\mathrm{Ra}\cdot\mathrm{Pr}}}\cdot\left[\left(1+\left|V^{n}_{i,j,k}\right|\cdot\frac{\sqrt{\mathrm{Ra}\cdot\mathrm{Pr}}\cdot h_y}{2}\right)^{-1}\frac{\Theta^{n+\frac{2}{3}}_{i,j+1,k}-2\cdot\Theta^{n+\frac{2}{3}}_{i,j,k}+\Theta^{n+\frac{2}{3}}_{i,j-1,k}}{h_y^2}\right], \tag{15}$$

$$\frac{\Theta^{n+1}_{i,j,k}-\Theta^{n+\frac{2}{3}}_{i,j,k}}{d\tau}+W^{n}_{i,j,k}\cdot\frac{\Theta^{n+1}_{i,j,k+1}-\Theta^{n+1}_{i,j,k-1}}{2\cdot h_z}-\left|W^{n}_{i,j,k}\right|\cdot\frac{\Theta^{n+1}_{i,j,k+1}-2\cdot\Theta^{n+1}_{i,j,k}+\Theta^{n+1}_{i,j,k-1}}{2\cdot h_z}=\frac{1}{\sqrt{\mathrm{Ra}\cdot\mathrm{Pr}}}\cdot\left[\left(1+\left|W^{n}_{i,j,k}\right|\cdot\frac{\sqrt{\mathrm{Ra}\cdot\mathrm{Pr}}\cdot h_z}{2}\right)^{-1}\frac{\Theta^{n+1}_{i,j,k+1}-2\cdot\Theta^{n+1}_{i,j,k}+\Theta^{n+1}_{i,j,k-1}}{h_z^2}\right]. \tag{16}$$

It was assumed that steady-state solution was found when the following convergence criteria were reached:

$$\left|\sqrt{\left(U^2+V^2+W^2\right)^{n+1}}-\sqrt{\left(U^2+V^2+W^2\right)^{n}}\right|<10^{-7},$$

$$\left|\Theta^{n+1}-\Theta^{n}\right|<10^{-7}.$$

2.7 Mesh refinement and validation

To obtain grid-independent results, spatial convergence should be performed before the main computations. The mesh was refined until discrepancy did not exceed 3%. Grid study for both the hybrid lattice Boltzmann model and pure finite difference approach is presented in Fig. 2.

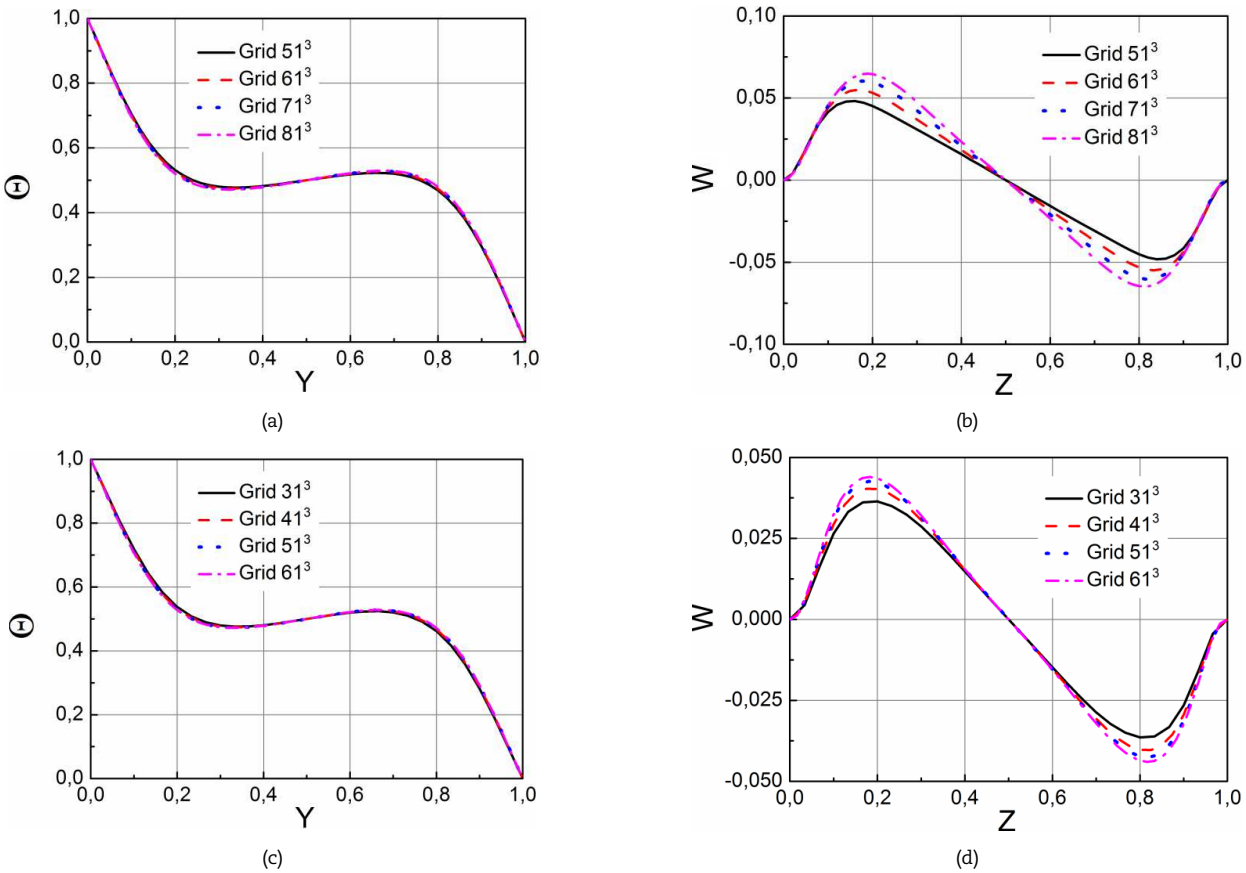

Fig. 2. Temperature (a, c) and velocity (b, d) profiles in the mid-plane when $Rd = 2$, $Ra = 10^5$ and $Pr = 0.71$: (a, b) LB-FDM, (c, d) pure FDM.

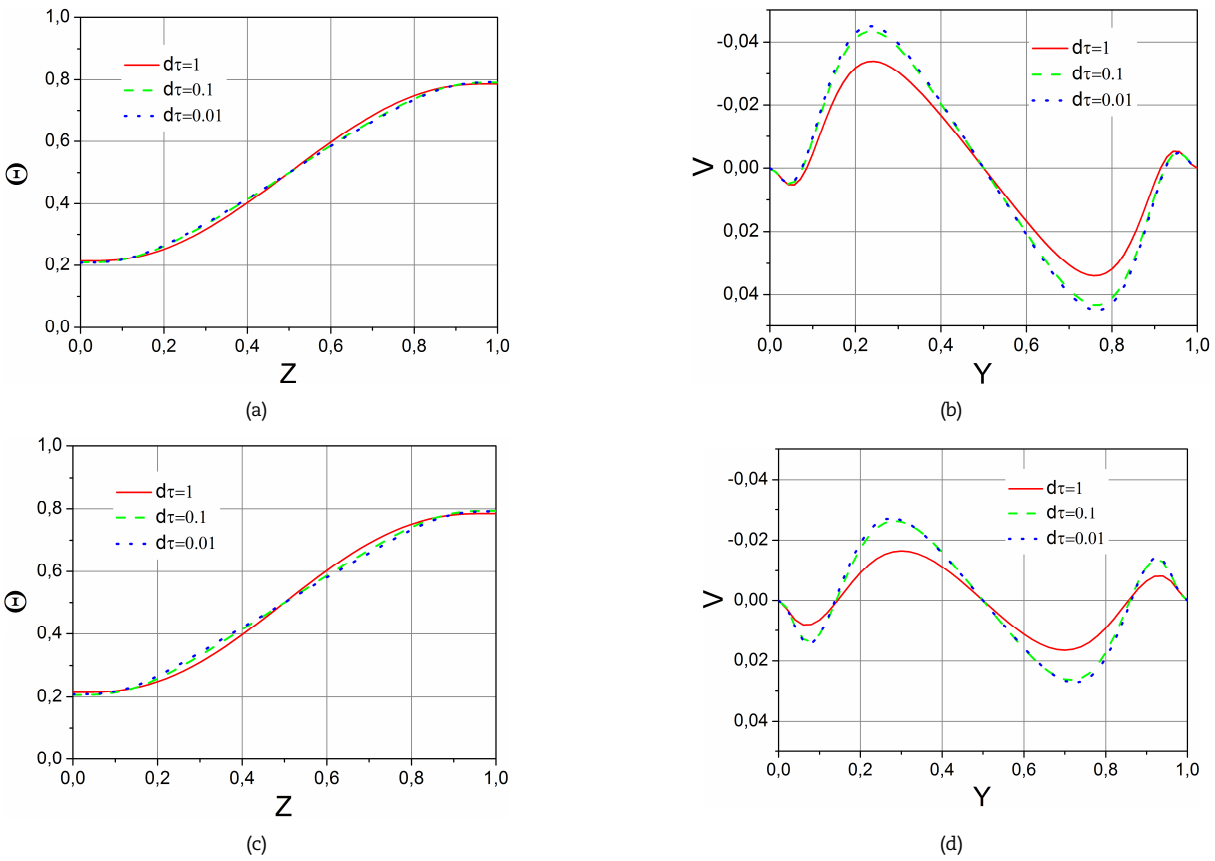

Fig. 3. Temperature (a, c) and velocity (b, d) profiles in the mid plane when Rd = 2, Ra = 10^5 and Pr = 0.71: (a, b) LB-FDM, (c, d) pure FDM.

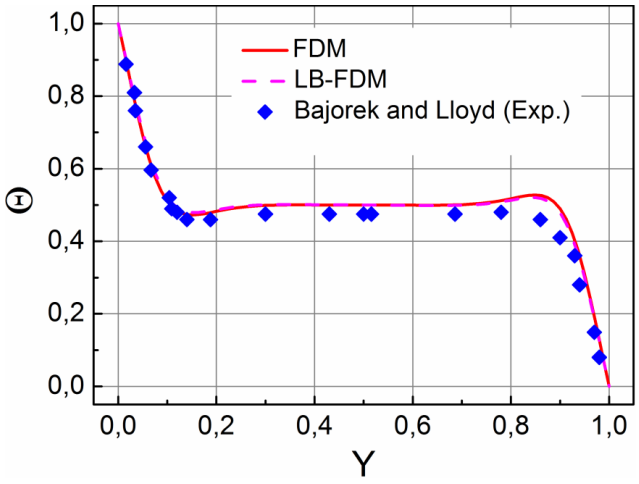

Fig. 4. Temperature variation in a closed differentially heated air-filled cube with Ra = 355700, Rd = 0 and Pr = 0.71.

It was interesting to note that temperature was insensitive to the grid density variation for both LB-FDM and pure FDM models. On the contrary, grid-independent values of velocity were obtained with the mesh size of 71^3 for the hybrid lattice Boltzmann and 51^3 for the vorticity-vector potential formulations.

The effect of the macroscopic time step on thermal and flow characteristics are studied and given in Fig. 3. It was found that temporal convergence was reached with $d\tau = 0.01$ both in the case of the hybrid lattice Boltzmann – finite difference method and pure finite difference technique. Thus, numerical study of 3D natural convection combined with Rosseland radiation was performed on a uniform grid of 71^3 nodes for the LB-FDM and 51^3 nodes for the pure FDM with the macroscopic time step of 0.01.

Developed numerical codes were validated against experimental [38] and numerical [39, 40] data of other researchers. Bajorek and Lloyd conducted experimental study of laminar natural convection in a closed differentially heated cavity. Figure 4 shows temperature variation in the mid-plane.

Natural convection in a closed box with differentially heated side walls is a classical benchmark problem which is well studied and used for validation of novel numerical techniques. Figure 5 shows three-dimensional thermal fields.

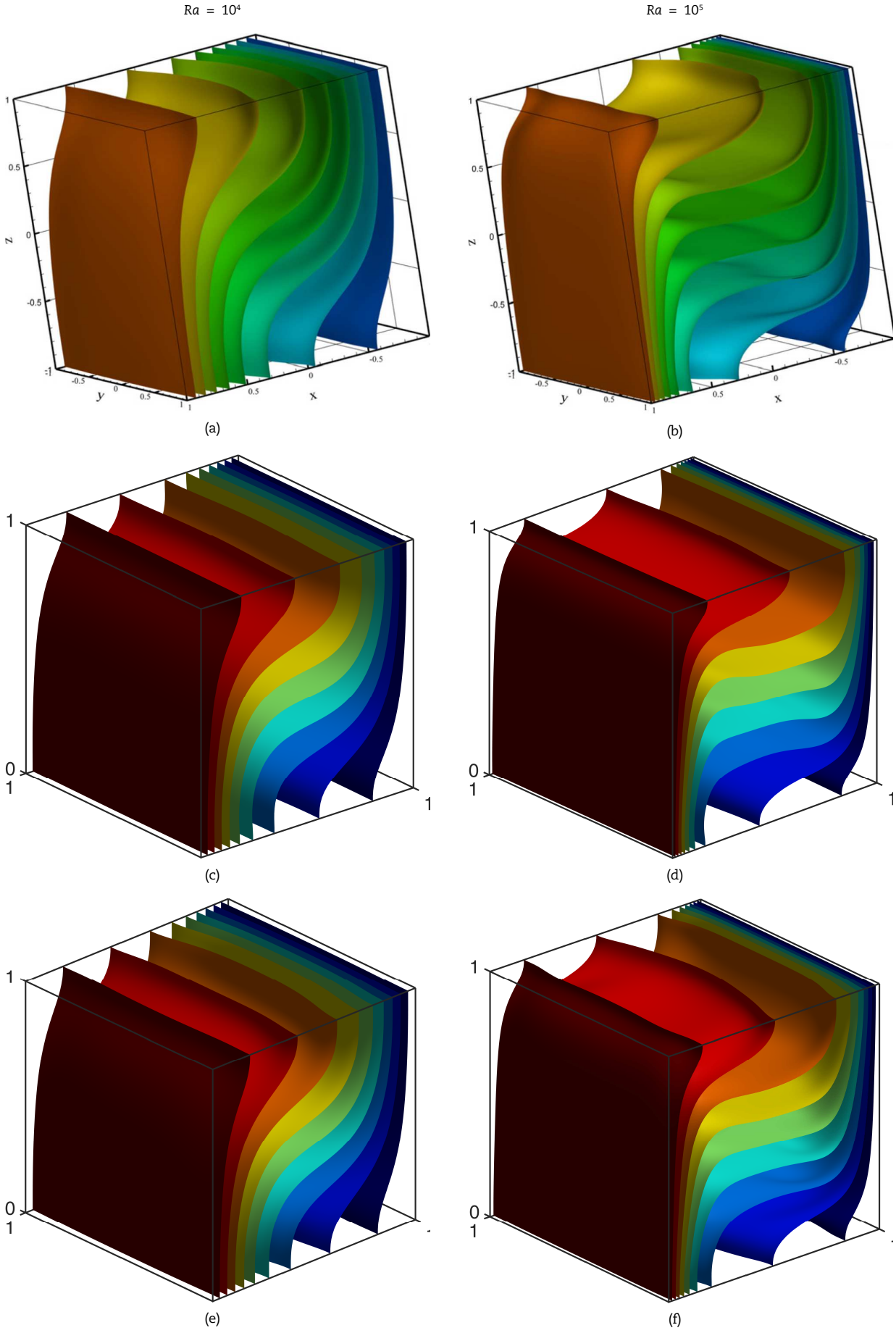

Fig. 5. Variation of temperature iso-surfaces with *Ra* when *Pr* = 0.71: (a, b) [28]; (c, d) FDM; (e, f) LB-FDM

Table 1. Variation of mean Nusselt numbers with the Rayleigh number

Ra	U				W				Nu			
	Ref. [39]	Ref. [40]	This study		Ref. [39]	Ref. [40]	This study		Ref. [39]	Ref. [40]	This study	
			FDM	LB-FDM			FDM	LB-FDM			FDM	LB-FDM
10^4	0.2013	0.1929	0.1835	0.1849	0.2252	0.222	0.2161	0.2164	2.1	2.065	2.147	2.126
10^5	0.1468	0.1389	0.1283	0.1283	0.2471	0.2466	0.2455	0.2437	4.361	4.378	4.418	4.329

Comparison of local and mean heat transfer and fluid flow characteristics is given in Table 1. It was found that local and mean heat transfer characteristics obtained with FDM and LB-FDM models were in a good agreement with experimental [38] and numerical [28, 39, 40] data of other researches. Thus, developed approaches can accurately simulate 3D natural convection in closed differentially heated cavities.

3. Results and Discussion

The radiatively participating fluid (water vapor) with the Prandtl number of 1 was considered. When conducting numerical study, the Rayleigh number was varied from 10^4 to 10^5 whereas variation range of radiation parameter was $0 \le Rd \le 4$. The main attention was given to comparative study of macroscopic and mesoscopic numerical techniques in terms of the 2D and 3D problem formulations. Along with that, computational performance of the hybrid lattice Boltzmann model is of great interest. Results of mathematical modelling are presented in terms of the temperature isosurfaces, velocity streamslices, temperature and velocity profiles, mean Nusselt numbers and running time columns.

3.1 Temperature and flow

Figure 6 presents temperature isosurfaces and velocity streamslices when varying the radiation parameter. It was found that volumetric radiation significantly altered temperature and flow pattern in the closed differentially heated cube. In the case of pure convection (Fig. 6 *a*), the fluid heated near the plane of $Y = 0$, $0 < X < 1$, $0 < Y < 1$ was ascended whereas the fluid cooled near the plane of $Y = 1$, $0 < X < 1$, $0 < Y < 1$ was descended. As a result, a large-scale vortex (Fig. 6 *d*) was formed in the cavity. Along with that, horizontal thermal stratification was observed in the cube. It should be noted that two secondary vortices were formed inside the large-scale convective cell due to a relatively strong buoyancy force. When taking into account Rosseland radiation (Fig. 6 *b*), the fluid was heated both by natural convection and volumetric radiation. A sharp increase in the temperature near the left wall in the case of pure convection was smoothed due to radiative heating of the fluid. Moreover, the thickness of boundary layer was increased and one-cellular flow pattern (Fig. 6 *e*) was formed. Probably, thermal radiation weakened natural convective mechanism of heat transfer. Further increase in the radiation parameter to 4 led an oblique stratification (Fig. 6 *c*). However, enhancement of volumetric radiation slightly altered the flow pattern and fluid flow became quasi two-dimensional in the closed differentially heated cube.

Figure 7 shows temperature profiles obtained with different numerical 2D and 3D techniques. Vorticity – stream function model and D2Q9 lattice Boltzmann scheme with the BGK approximation were used for two-dimensional simulations. For these cases, numerical procedure can be found in previous works [41, 42].

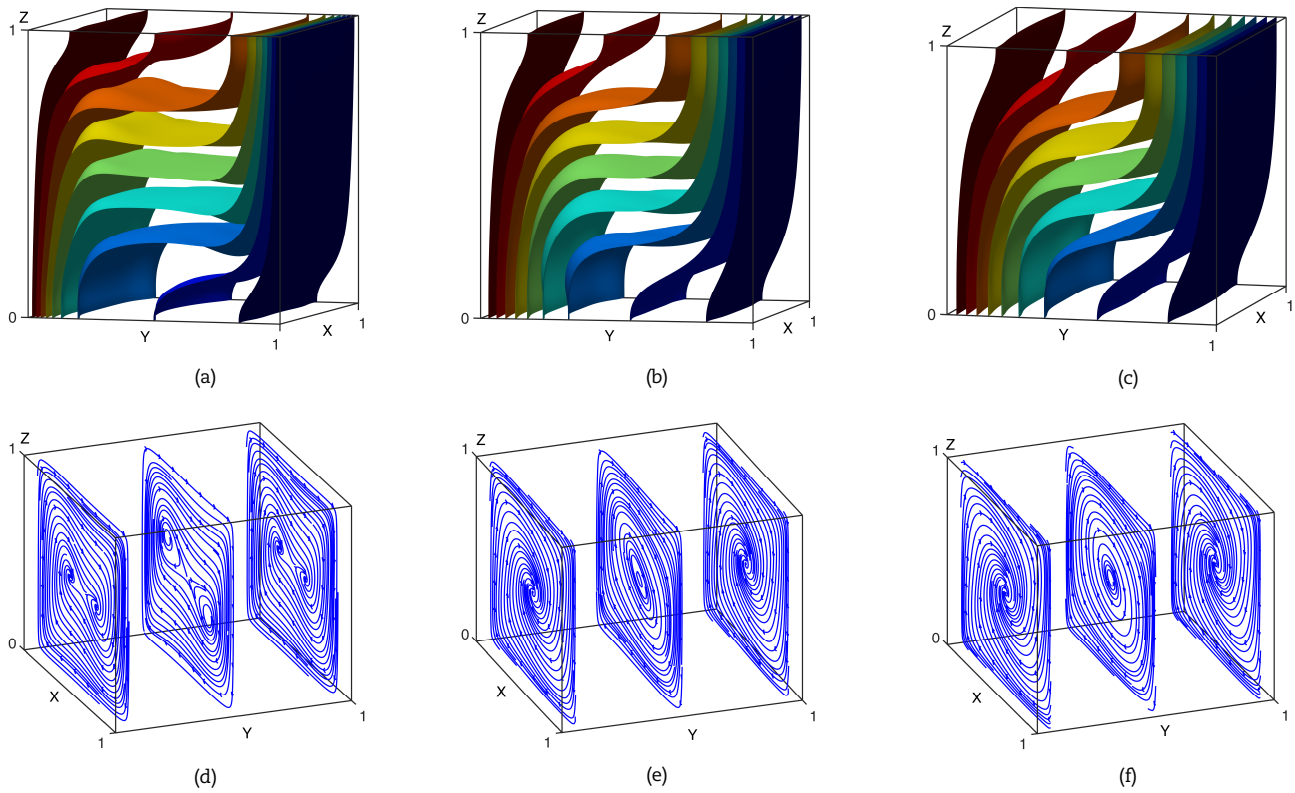

Fig. 6. Steady-state temperature isosurfaces (a, b, c) and velocity streamslices (d, e, f) when $Ra = 10^5$ and $Pr = 1$: (a, d) pure convection; (b, e) $Rd = 2$; (c, f) $Rd = 4$.

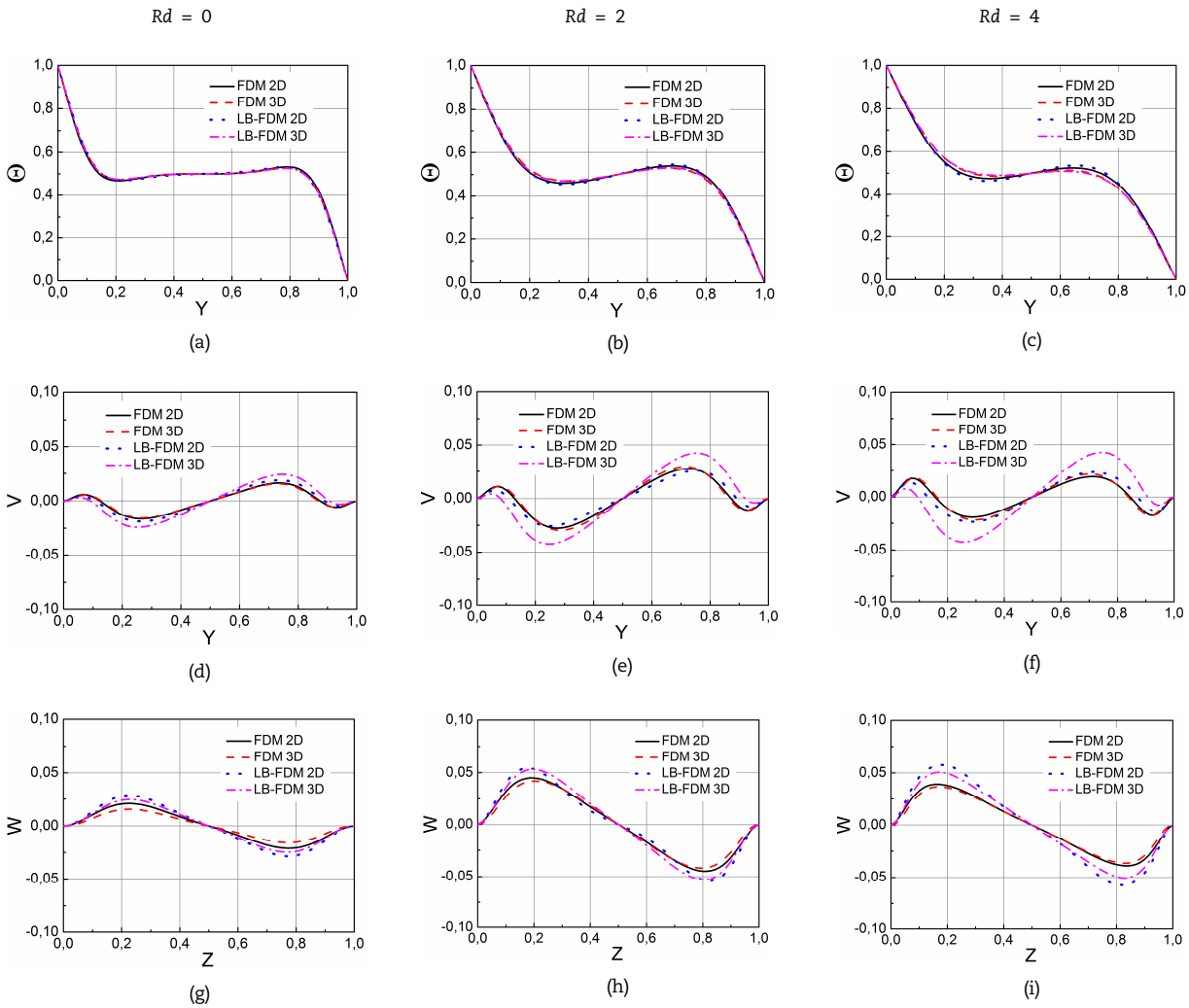

Fig. 7. Temperature (a, b, c) and velocity (d, e, f, g, h, i) profiles when $Ra = 10^5$ and $Pr = 1$ in the mid-plane and section of: (a, b, c, d, e, f) Z = 0.5; (g, h, i) Y = 0.5.

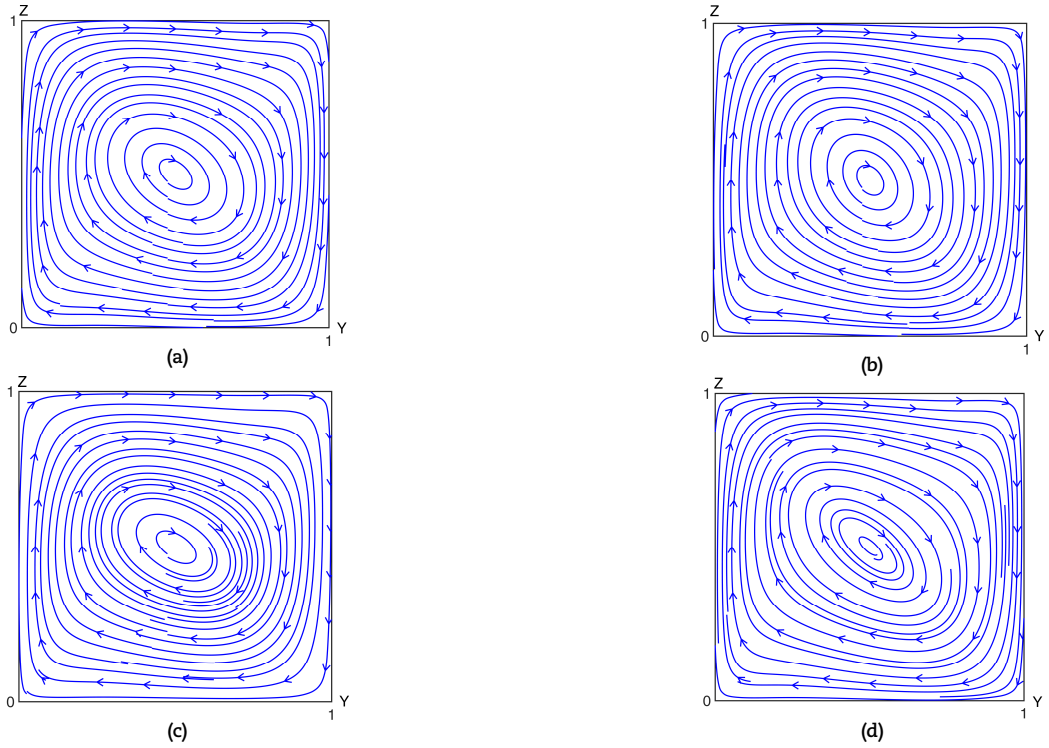

Fig. 8. Velocity streamslices in the mid-plane when $Ra = 10^5$, $Rd = 2$ and $Pr = 1$: (a) FDM 2D; (b) LB-FDM 2D; (c) FDM 3D; (d) LB-FDM 3D.

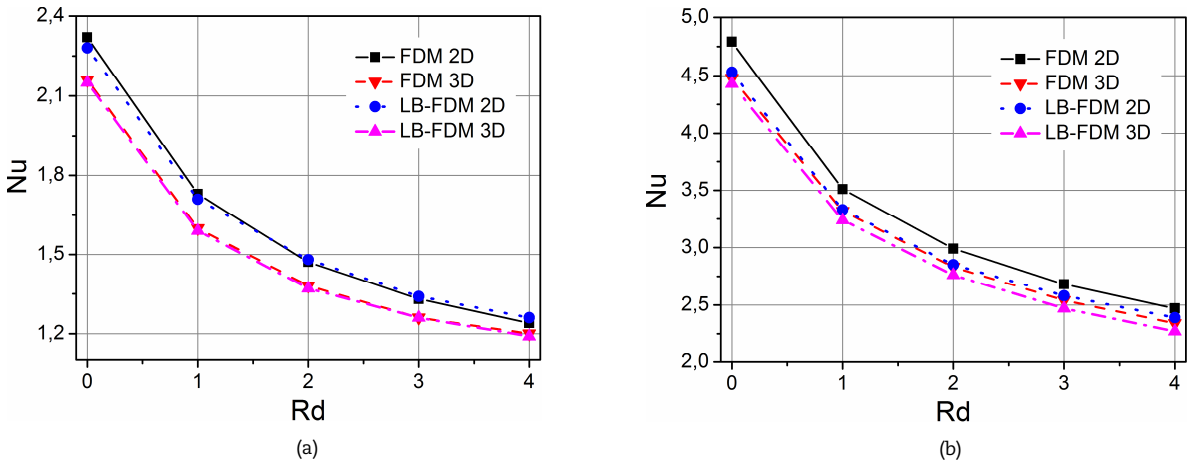

Fig. 9. Variation of mean convective Nusselt numbers with radiation parameter when $Pr = 0.71$: (a) $Ra = 10^4$; (b) $Ra = 10^5$.

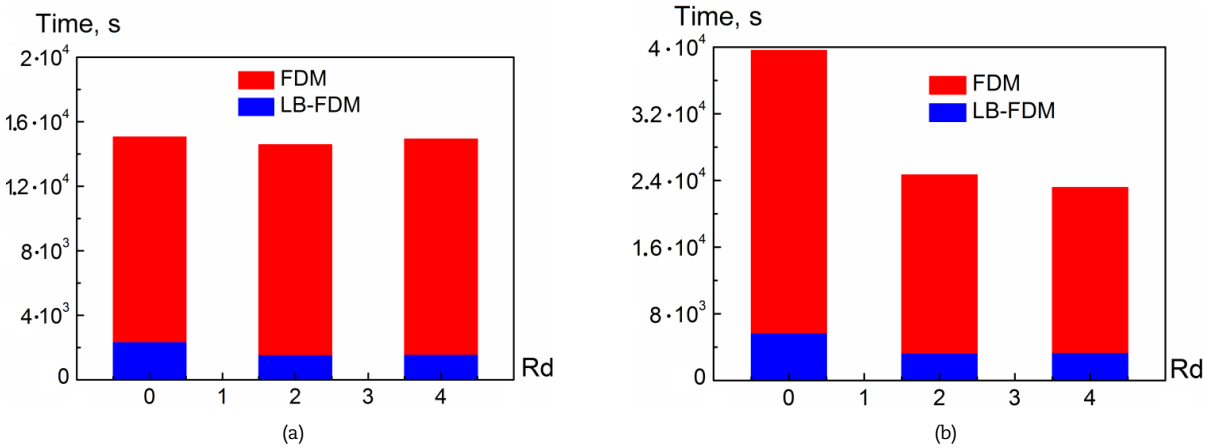

Fig. 10. Variation of running times with radiation parameter when $Pr = 0.71$: (*a*) $Ra = 10^4$; (*b*) $Ra = 10^5$.

It was found that both LB-FDM and pure FDM techniques produced the same values of temperature when varying the radiation parameter. Moreover, a transition from a horizontal thermal stratification to an oblique stratification was clearly observed (Fig. 7 *a, b, c*) when taking into account volumetric radiation. Along with that, the temperature near the hot/cold walls was increased/decreased with an increment in the radiation parameter. This regularity was associated with an increase in the thickness of boundary layer with an enhancement in the volumetric radiation. Essentially, results obtained with 2D and 3D models well correlated in terms of the temperature. On the contrary, discrepancy in the velocity components between the hybrid lattice Boltzmann method and the vorticity – vector potential formulation was clearly observed. However, both 2D and 3D models produced the same trend of velocity. In the case of pure convection (Fig. 6 *d, g*), error in the values of velocity was insignificant. On the other hand, deviation in results obtained numerically by the LB-FDM and pure FDM approaches was increased with an enhancement in the Rosseland radiation. Moreover, the hybrid lattice Boltzmann model produced higher values of velocity in all cases under study. It was found that both 2D and 3D models based on pure finite difference techniques reproduced almost the same values of velocity when taking into account volumetric radiation. On the contrary, a significant discrepancy was observed in the velocity obtained with 2D and 3D hybrid lattice Boltzmann method.

Since discrepancy in local velocities obtained with models under study was found, flow pattern is of interest. Velocity streamslices in the mid-plane are presented in Fig. 8.

As mentioned earlier, the fluid heated near the left wall formed an up-ward flow and the fluid cooled near the right wall formed a down-ward flow. When taking into account Rosseland thermal radiation, flow pattern slightly altered with variation of numerical techniques. Generally, one-cellular fluid flow was created in all cases under consideration. Thus, it was interesting to note that an identical flow structures were formed despite the discrepancy in the values of velocity obtained with four different problem formulations. Probably, this regularity was associated with the same trends of velocity curves for pure FDM and LB-FDM under two- and three dimensional problem statement.

3.2 Heat transfer rate

When analyzing convective heat transfer, mean Nusselt number is of great importance. This dimensionless criterion is used in order to estimate the heat transfer rate. Figure 9 shows variation of mean convective Nusselt numbers with radiation parameter.

As could be assumed, an increment in the Rayleigh number led an enhancement of convective heat transfer rate since buoyancy driven flow was intensified. On the contrary, Rosseland radiation weakened natural convection. It should be noted that higher values of Nusselt numbers were observed for 2D models since heat transfer rate from a boundary was higher than from a plane. When $Ra = 10^4$ (Fig. 9 *a*), three-dimensional hybrid lattice Boltzmann and pure finite difference techniques reproduced the same values of *Nu*. Along with that, an error in the mean convective Nusselt numbers obtained with two-dimensional problem formulation was insignificant. The same regularity was observed when the Rayleigh number was increased to 10^5 (Fig. 9 *b*). Moreover, discrepancy in the *Nu* was lower when varying the numerical techniques with this value of *Ra*. However, in this case, the highest mean convective Nusselt numbers were obtained with 2D model based on pure finite difference method. To sum up, the results of integral analysis were in a very good agreement for both FDM and LB-FDM approaches.

3.3 Numerical performance

The lattice Boltzmann theory states that this mesoscopic approach is 20-40% faster than macroscopic methods based on Navier-Stokes equations. Indeed, this is a reasonable conclusion since there is no stationary mass conservation equation in the LBM. However, an accurate assessment of the lattice Boltzmann and conventional CFD techniques has not performed in terms of three-dimensional natural convection combined with thermal radiation. Thus, comparative study of 3D LB-FDM and pure FDM by means of the running time will be conducted in this sub-section.

Numerical codes based on the hybrid lattice Boltzmann and vorticity-vector potential formulations were both written in MATLAB R2017a. The Intel Core i5-4440 was used for all cases under consideration without parallel implementation. Computational performance was analyzed in terms of the running times. The tic-toc function was used in order to estimate computational time required to obtain the steady-state grid-independent solutions. Figure 10 presents variation of running times with radiation parameter.

As could be assumed, computational performance of the hybrid lattice Boltzmann method was several times higher than pure finite difference technique based on the vorticity-vector potential formulation. An increment in the Rayleigh number led to an increase in the running times of LB-FDM and FDM models since natural convection was enhanced with a growth in the buoyancy force. When $Ra = 10^4$ (Fig. 10 *a*), running times were slightly altered with variation of radiation parameter for both hybrid and pure finite difference approaches. However, the time needed to reach steady-state grid-independent solution was approximately 10 times lower in the case of LB-FDM and $Rd = 4$. On the other hand, characteristic criterion under study was significantly reduced when taking into account thermal radiation in the case of $Ra = 10^5$. This regularity was probably associated with a decrease in the natural convective heat transfer rate with an enhancement of Rosseland radiation. Thus, the intensity of currents was lowered and flow became steady faster. To summarize the above, it was clearly seen that numerical efficiency of the hybrid lattice Boltzmann method was significantly better than conventional CFD approach. It should be noted that a number of nodes for LB-FDM was 357911 and grid size of 132651 was used for pure finite difference method. And even in this case, running times of the hybrid model were more than 7 times less. Primarily, solution of three steady vector potential equations at every time step consumed a lot of time.

4. Conclusion

Three-dimensional natural convection combined with Rosseland radiation was numerically examined in terms of the mesoscopic and macroscopic simulation. Comparative study of 2D and 3D problem formulations was performed. The main findings are as follows:

- When taking into account Rosseland radiation, the fluid flow became one-cellular and quasi two-dimensional. The hybrid lattice Boltzmann and vorticity-vector potential formulations reproduced the same values of temperature obtained with 2D and 3D models. However, a significant discrepancy was found in local velocities. Along with that, the same trend of velocity curves was observed for all cases under consideration. Therefore, identical flow pattern was formed despite the discrepancy in the values of velocity obtained with four different problem formulations.
- Natural convective heat transfer rate was reduced as Rosseland radiation was enhanced. Thus, the mean convective Nusselt number was a decreasing function of radiation parameter whereas an increment in the Rayleigh number increased dimensionless heat transfer coefficient. When analyzing the integral characteristics, it was found that mean Nusselt numbers obtained with the hybrid mesoscopic and macroscopic models were in a satisfactory agreement for both 2D and 3D problem formulations.
- Rosseland radiation reduced running times for both LB-FDM and FDM models. Generally, the overall numerical performance of the hybrid lattice Boltzmann method was significantly better than conventional CFD approach. When $Ra=10^5$ and $Rd=4$, running time of pure FDM was 7 times higher while the number of nodes was approximately 2.5 lower.

Author Contributions

All parts of the paper were written by Alexander Nee

Acknowledgments

The author would like to acknowledge the very competent Reviewers for their careful evaluation of the manuscript, valuable comments and suggestions.

Conflict of Interest

The author declares no potential conflicts of interest concerning the research, authorship, and publication of this article.

Funding

The work was supported by the Russian Science Foundation (the grant number № 21-79-00011).

Data Availability Statements

The datasets generated and/or analyzed during the current study are available from the corresponding author on a reasonable request.

Nomenclature

a	Thermal diffusivity [m^2/s]	T	Temperature [K]
a_R	Rosseland mean absorption coefficient [1/m]	T_0	Initial temperature [K]
c	Lattice speed [m/s]	T_c	Temperature of the cold wall [-]
c_k	Particle speeds [m/s]	T_h	Temperature of the hot wall [-]
f	Distribution function [kg/m^3]	w_k	Weighting factor

F	Force, [kg/(s m^3)]
g	Gravitational acceleration [m/s^2]
h	Dimensionless spatial step [-]
L	Length of the cavity [m]
Nu	Mean convective Nusselt number [-]
Pr	Prandtl number [-]
R	Universal gas constant [J/(K mole)]
Rd	Radiation parameter [-]
t	Time [s]
t_0	Time scale [s]
Δt	Time step in the lattice Boltzmann equation [s]
u,v,w	Velocity vector components [m/s]
U,V,W	Dimensionless analogies of u, v, w [-]
V_{nc}	Velocity scale [m/s]
x,y,z	Cartesian coordinates [m]
X,Y,Z	Dimensionless analogies of x, y, z [-]

Greek symbols

β	Thermal expansion [1/K]
λ	Heat conductivity [W/(m K)]
Θ	Dimensionless temperature [-]
ν	Kinematic viscosity [m^2/s]
ρ	Density [kg/m^3]
σ	Stefan-Boltzmann constant [W/(m^{2}K^4)]
τ	Dimensionless time [-]
$d\tau$	Dimensionless macroscopic time step [-]
ω	Vorticity [1/s]
Ω	Dimensionless analogue of ω
ξ	Relaxation frequency [1/s]
ψ	Vector potential [m^2/s]
Ψ	Dimensionless analogue of ψ

References

[1] Akiyama, M., Chong, Q.P., Numerical analysis of natural convection with surface radiation in a square enclosure, *Numer. Heat Tr. A-Appl.*, 32, 1997, 419–433. http://dx.doi.org/10.1080/10407789708913899

[2] Bouafia, M., Hamimid, S., Guellal, M., Non-Boussinesq convection in a square cavity with surface thermal radiation, *Int. J. Therm. Sci.*, 96, 2015, 236–247. https://doi.org/10.1016/j.ijthermalsci.2015.04.017

[3] Wang, H., Xin, S., Le Quere, P., Etude numerique du couplage de la convection naturelle avec le rayonnement de surfaces en cavite carree remplie d'air, *Comptes Rendus Mecanique*, 334, 2006, 48–57. https://doi.org/10.1016/j.crme.2005.10.011

[4] Ashish Gad, M., Balaji, C., Effect of surface radiation on RBC in cavities heated from below, *Int. Commun. Heat. Mass.*, 37, 2010, 1459–1464. https://doi.org/10.1016/j.icheatmasstransfer.2010.08.003

[5] Xaman, J.P., Hinojosa, J.F., Flores, J.J., Cabanillas, R.E., Effect of the surface thermal radiation on turbulent natural convection in tall cavities of facade elements, *Heat Mass Transfer*, 45, 2008, 177–185. https://doi.org/10.1007/s00231-008-0393-5

[6] Ibrahim, A., Saury, D., Lemonnier, D., Coupling of turbulent natural convection with radiation in an air-filled differentially-heated cavity at Ra = 1.5×109, *Comput. Fluids*, 88, 2013, 115–125. https://doi.org/10.1016/j.compfluid.2013.09.006

[7] Wu, T., Lei, C., On numerical modelling of conjugate turbulent natural convection and radiation in a differentially heated cavity, *Int. J. Heat Mass Tran.*, 91, 2015, 454–466. https://doi.org/10.1016/j.ijheatmasstransfer.2015.07.113

[8] Sharma, A.K., Velusamy, K., Balaji, C., Venkateshan, S.P., Conjugate turbulent natural convection with surface radiation in air filled rectangular enclosures, *Int. J. Heat Mass Trans.*, 50, 2007, 625–639. https://doi.org/10.1016/j.ijheatmasstransfer.2006.07.022

[9] Ridouane, E.H., Hasnaoui, M., Campo, A., Effects of surface radiation on natural convection in a Rayleigh-Benard square enclosure: steady and unsteady conditions, *Heat Mass Transfer*, 42, 2006, 214–225. https://doi.org/10.1007/s00231-005-0012-7

[10] Lari, K., Baneshi, M., Gandjalikhan Nassab, S.A., Komiya, A., Maruyama, S., Combined heat transfer of radiation and natural convection in a square cavity containing participating gases, *Int. J. Heat Mass Trans.*, 54, 2011 5087–5099. https://doi.org/10.1016/j.ijheatmasstransfer.2011.07.026

[11] Ibrahim, A., Lemonnier, D., Numerical study of coupled double-diffusive natural convection and radiation in a square cavity filled with A N2–CO2 mixture, *Int. Commun. Heat. Mass.*, 36, 2009, 197–202. https://doi.org/10.1016/j.icheatmasstransfer.2008.10.019

[12] Naceur Borjinia, M., Ben Aissia, H., Halouani, K., Zeghmati, B., Effect of radiative heat transfer on the three-dimensional Buoyancy flow in cubic enclosure heated from the side, *Int. J. Heat Fluid Flow*, 29, 2008, 107–118. https://doi.org/10.1016/j.ijheatfluidflow.2007.07.012

[13] Cherifi, M., Laouar-Meftah, S., Benbrik, A., Lemonnier, D., Saury, D., Interaction of radiation with double-diffusive natural convection in a three-dimensional cubic cavity filled with a non-gray gas mixture in cooperating cases, *Numer. Heat Tr. A-Appl.*, 69, 2016, 479–496. https://doi.org/10.1080/10407782.2015.1090233

[14] Al-Rashed, A., Kolsi, L., Tashkandi, M.A., Malekshah, E.H., Chamkha, A.J., Borjini, M.N., Three-dimensional combined radiation-magnetoconvection of low electrically conductive dielectric oxide melt, *Int. J. Numer. Method Heat Fluid Flow,* 29, 2019, 3611-3637. https://doi.org/10.1108/HFF-06-2018-0263

[15] Abidi, A., Kolsi, L., Borjini, M.N., Ben Aissia, H., Effect of Radiative Heat Transfer on Three-Dimensional Double Diffusive Natural Convection, *Numer. Heat Tr. A-Appl.*, 60, 2011, 785–809. https://doi.org/10.1080/10407782.2011.627797

[16] Vivek, V., Sharma, A.K., Balaji, C., Interaction effects between laminar natural convection and surface radiation in tilted square and shallow enclosures, *Int. J. Therm. Sci.*, 60, 2012, 70–84. https://doi.org/10.1016/j.ijthermalsci.2012.04.021

[17] Moufekkir, F., Moussaoui, M.A., Mezrhab, A., Bouzidi, M., Laraqi, N., Study of double-diffusive natural convection and radiation in an inclined cavity using lattice Boltzmann method, *Int. J. Therm. Sci.*, 63, 2013, 65–86. https://doi.org/10.1016/j.ijthermalsci.2012.07.015

[18] Liu, Y., Phan-Thien, N., A complete conjugate conduction convection and radiation problem or a heated block in a vertical differentially heated square enclosure, *Comput. Mech.*, 24, 1999, 177–186. https://doi.org/10.1007/s004660050450

[19] Saravanan, S., Sivaraj, C., Combined natural convection and thermal radiation in a square cavity with a nonuniformly heated plate, *Comput. Fluids,* 117, 2015, 125–138. https://doi.org/10.1016/j.compfluid.2015.05.005

[20] Patil, S., Sharma, A.K., Velusamy, K., Conjugate laminar natural convection and surface radiation in enclosures: Effects of protrusion shape and position, *Int. Commun. Heat. Mass. Trans.*, 76, 2016, 139–146. https://doi.org/10.1016/j.icheatmasstransfer.2016.05.006

[21] Xin, S., Salat, J., Joubert, P., Sergent, A., Penot, F., Le Quéré, P., Resolving the stratification discrepancy of turbulent natural convection in differentially heated air-filled cavities. Part III: A full convection–conduction–surface radiation coupling, *Int. J. Heat Fluid Flow*, 42, 2013, 33–48. https://doi.org/10.1016/j.ijheatfluidflow.2013.01.021

[22] Martyushev, S.G., Sheremet, M.A., Conjugate natural convection combined with surface thermal radiation in an air filled cavity with internal heat source, *Int. J. Therm. Sci.*, 76, 2014, 51–67. https://doi.org/10.1016/j.ijthermalsci.2013.08.012

[23] Martyushev, S.G., Sheremet, M.A., Conjugate natural convection combined with surface thermal radiation in a three-dimensional enclosure with a heat source, *Int. J. Heat Mass Trans.*, 73, 2014, 340–353. https://doi.org/10.1016/j.ijheatmasstransfer.2014.02.009

[24] Arun, S., Satheesh, A., Chamkha, A.J., Numerical Analysis of Double-Diffusive Natural Convection in Shallow and Deep Open-Ended Cavities Using Lattice Boltzmann Method, *Arab. J. Sci. Eng.*, 45, 2020, 861–876. https://doi.org/10.1007/s13369-019-04156-3

[25] Hammouda, S., Amami, B., Dhahri, H., Viscous dissipation effects on heat transfer for nanofluid flow over a backward-facing step through porous medium using lattice boltzmann method, *J. Nanofluids*, 7, 2018, 668–682. https://doi.org/10.1166/jon.2018.1491

[26] Lallemand, P., Lou, L.-S., Hybrid finite-difference thermal lattice Boltzmann equation, *Int. J. Modern Physics B,* 17, 2003, 41–47.

[27] Moufekkir, F., Moussaouia, M.A., Mezrhab, A., Bouzidi, M., Laraqi, N., Study of double-diffusive natural convection and radiation in an inclined cavity using lattice Boltzmann method, *Int. J. Therm. Sci.,* 63, 2013, 65–86. https://doi.org/10.1016/j.ijthermalsci.2012.07.015

[28] Obrecht, C., Kuznik, F., Tourancheau, B., Roux, J.-J., The LMA project: A thermal lattice Boltzmann solver for the GPU, *Comput. Fluids*, 54, 2012, 118–126. https://doi.org/10.1016/j.compfluid.2011.10.011

[29] Benhamou, J., Jami, M., Three-dimensional numerical study of heat transfer enhancement by sound waves using mesoscopic and macroscopic approaches, *Heat Transfer*, 2022. https://doi.org/10.1002/htj.22482

[30] Nee, A., Hybrid lattice Boltzmann—Finite difference formulation for combined heat transfer problems by 3D natural convection and surface thermal radiation, *Int. J. Mech. Sci.,* 173, 2020, 105447. https://doi.org/10.1016/j.ijmecsci.2020.105447

[31] Chen, Y., Xie, X., Vorticity vector-potential method for 3D viscous incompressible flows in time-dependent curvilinear coordinates, *J. Comput. Phys.*, 312, 2016, 50–81. https://doi.org/10.1016/j.jcp.2016.02.020

[32] Bondareva, N.S., Sheremet, M.A., 3D natural convection melting in a cubical cavity with a heat source, *Int. J. Therm. Sci.*, 115, 2017, 43–53. https://doi.org/10.1016/j.ijthermalsci.2017.01.021
[33] Magyari, E., Pantokratoras, A., Note on the effect of thermal radiation in the linearized Rosseland approximation on the heat transfer characteristics of various boundary layer flows, *Int. Commun. Heat Mass Trans.*, 38, 2011, 554–556. https://doi.org/10.1016/j.icheatmasstransfer.2011.03.006
[34] Sheremet, M.A., Pop, I., Natural convection combined with thermal radiation in a square cavity filled with a viscoelastic fluid, *Int. J. Numer. Method Heat Fluid Flow,* 28, 2018, 624-640. https://doi.org/10.1108/HFF-02-2017-0059
[35] Succi, S., *The Lattice Boltzmann Equation for Fluid Dynamics and Beyond*, Oxford University Press, 2001.
[36] Samarskii, A.A., *The theory of difference schemes* [in Russian], Nauka, Moscow, 1977.
[37] Roache, P.J., *Computational Fluid Dynamics*, Hermosa Publishers, Albuquerque, 1976.
[38] Bajorek, S.M., Lloyd, J.R., Experimental investigation of natural convection in partitioned enclosures, *J. Heat Transf.*, 104, 1982, 527–532. https://doi.org/10.1115/1.3245125
[39] Fusegi, T., Hyin, J.M., Kuwahara, K., A numerical study of three-dimensional natural convection in a differentially heated cubical enclosure, *Int. J. Heat Mass Trans.*, 34, 1991, 1543–1557. https://doi.org/10.1016/0017-9310(91)90295-P
[40] Astanina, M.S., Buonomo, B., Manca, O., Sheremet, M.A., Effect of third size on natural convection of variable viscosity fluid in a closed, *Int. Commun. Heat Mass Trans.*, 128, 2021, 105618. https://doi.org/10.1016/j.icheatmasstransfer.2021.105618
[41] Kuznetsov, G.V., Kurilenko, N.I., Nee, A.E., Mathematical modelling of conjugate heat transfer and fluid flow inside a domain with a radiant heating system, *Int. J. Therm. Sci.*, 131, 2018, 27–39. https://doi.org/10.1016/j.ijthermalsci.2018.05.010
[42] Nee, A.É., Hybrid Approach to Modeling the Process of Convective Radiative Heat and Mass Transfer in Closed Differentially Heated Cavities, *J. Eng. Phys. Thermophys.*, 94, 2021, 1008–1019. https://doi.org/10.1007/s10891-021-02378-7

ORCID iD

Alexander Nee https://orcid.org/0000-0002-7928-0329

How to cite this article: Nee A. Comparative Study of Hybrid Lattice Boltzmann and Vorticity-vector Potential Modelling of 2D and 3D Natural Convection Combined with Rosseland Radiation, *J. Appl. Comput. Mech.*, 8(4), 2022, 1467–1479. https://doi.org/10.22055/jacm.2022.40276.3550